

YANGCHUN HAN*, JIULONG CHENG*[#], QISONG HUANG*,
D.H.STEVE ZOU**, JIN ZHOU*, SHAOHUA HUANG*, YUN LONG*

**PREDICTION OF THE HEIGHT OF OVERBURDEN FRACTURED ZONE IN DEEP COAL MINING:
CASE STUDY**

**PROGNOZOWANIE WYSOKOŚCI STREFY SPĘKAŃ W WARSTWACH NADKŁADU
W PODZIEMNYCH KOPALNIACH WĘGLA: STUDIUM PRZYPADKU**

In the process of coal extraction, a fractured zone is developed in the overburden above the goaf. If the fractured zone is connected with an aquifer, then water inrush may occur. Hence, research and analysis of the height of overburden fractured zone (HOFZ) are of considerable significance. This study focuses on the HOFZ determination in deep coal mining. First, general deformation failure characteristics of overburden were discussed. Second, a new method, numerical simulation by orthogonal design (NSOD), have been proposed to determinate the HOFZ in deep coal mining. Third, the validity of NSOD is verified in the practical application, compared with empirical formula in Chinese Regulations and in-situ test. These three methods were applied to determine the HOFZ of working face No. 111303 in No. 5 coal mine. The predicted HOFZ of NSOD is found to be similar to the result of the in-situ test (8.9% relative error), whereas the HOFZ calculated by the empirical formula has extremely large error (25.7% relative error). Results show that the NSOD can reliably predict the HOFZ in deep coal mining and reduce time and expenses required for in-situ test.

Keywords: the height of overburden fractured zone, numerical simulation, orthogonal design, in-situ test

W trakcie prowadzenia wydobycia węgla w warstwie skalnej leżącej ponad zrobami powstaje strefa spękań. Jeśli nieciągłości te związane są z formacjami wodonośnymi, może nastąpić nagły wypływ wód do kopalni. Stąd też waga problemu i konieczność badania wysokości strefy spękań w warstwach nadkładu zalegających nad wyrobiskiem. W pracy tej główny nacisk położono na określenie wysokości strefy spękań warstwy nadkładu zalegającej ponad wyrobiskiem w kopalni podziemnej. W pierwszej części pracy przedstawiono główne charakterystyki powstawania deformacji i pęknięć w warstwach nadkładu. Następnie zaproponowano nową metodę symulacji numerycznych w układzie ortogonalnym i jej wykorzystanie do określania wysokości strefy spękań w warstwach nadkładu w kopalni podziemnej.

* COLLEGE OF GEOSCIENCE AND SURVEYING ENGINEERING, CHINA UNIVERSITY OF MINING AND TECHNOLOGY (BEIJING), BEIJING 100083, CHINA

** DEPARTMENT OF CIVIL AND RESOURCE ENGINEERING, DALHOUSIE UNIVERSITY, HALIFAX, CANADA

Corresponding author: JLCheng@cumtb.edu.cn

Następnie powyższą metodę zweryfikowano w praktycznym zastosowaniu, jako poziomy odniesienia wykorzystano odpowiednie wzory empiryczne określone w przepisach obowiązujących w Chinach oraz wyniki pomiarów in-situ. Powyższe trzy metody zastosowane zostały do określenia wysokości strefy spękań w warstwach nadkładu przy prowadzeniu ściany 111303 w kopalni węgla nr 5. Wyniki obliczeń wysokości strefy spękań uzyskane w oparciu o zaproponowaną nową metodę w dużym stopniu pokrywały się z wynikami pomiarów in-situ (błąd względny 8.9%); podczas gdy obliczenia wysokości strefy spękań w oparciu o odpowiednie wzory empiryczne obarczone były dużym błędem (błąd względny 25.7%). Uzyskane wyniki wskazują wiarygodność obliczeń w oparciu o zaproponowaną metodę, co pozwoli na ograniczenie czasu i kosztów związanych z wykonywaniem pomiarów in-situ.

Słowa kluczowe: wysokość strefy spękań w warstwie nadkładu, symulacje numeryczne, układ ortogonalny, pomiar in-situ

1. Introduction

Coal mining may cause overburden failure and result in fractured zone. The distribution range of the fractured zone is related to the safety of mine. If the fractured zone is connected with an aquifer, then water inrush disaster may occur. Simultaneously, the range of fractured zone determines the drilling design for gas drainage.

Singh et al. (1983) divided the overburden movement area into three zones (Fig. 1): the lower part is the caving zone, the middle part is the fractured zone, and the upper part is the continuous deformation zone. Cracks and voids in the caving and fractured zones may connect the working face with aquifer and pose water hazard threat to mining.

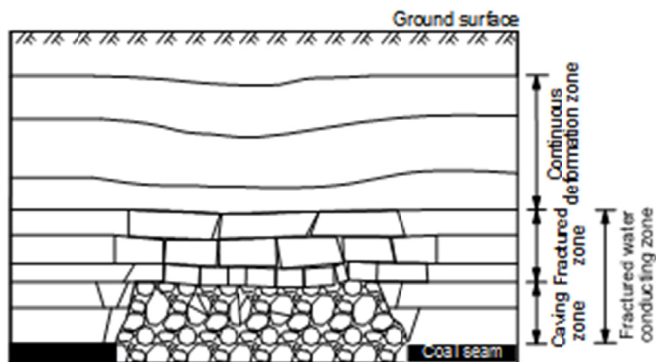


Fig. 1. Three zones of overburden movement area

The height of overburden fractured zone (HOFZ) has always been the study emphasis of overburden failure mechanism. Measures of numerical simulation, in-situ test, and empirical formula calculation were used to predict the HOFZ in numerous literature. Wang et al. (2016) dealt with the relationship between the HOFZ and the strain of overlying rock strata to guide methane drainage. Miao et al. (2011) studied the overburden failure mechanism through surface borehole hydrological observation and similar simulation test in Bulianta Coal Mine, and analyzed the impact of key strata on the HOFZ. Zhang et al. (2004) analyzed the HOFZ of working face 102 in Daliuta Coal Mine through ground borehole hydrological observation and numerical

simulation. Zhang et al. (2011) studied the mining-induced overburden failure in shallow coal mining via in-situ test and surface borehole hydrological observation. Xu et al. (2010) combined numerical simulation results with geophysical methods and in-situ test to study the HOFZ under the Xiaolangdi Reservoir.

The in-situ test can obtain an accurate result but is limited by complicated craft and inflated cost simultaneously. Therefore, combined with in-situ test data, numerous researchers established a series of empirical formulas to calculate the HOFZ. Peng et al. (1992) and Zhou (1991) established relevant empirical formula considering the relationship between coal mining thickness and the HOFZ. Majdi et al. (2012) proposed five formulas to calculate the HOFZ by analyzing the geometry characteristics of fractured zone after coal mining. In addition, numerical and physical models were widely used to determine the HOFZ (Ghabraie et al., 2015; Singh et al., 2009; Sui et al., 2015; Xie et al., 2009).

These studies are of considerable significance for understanding the mechanism of overburden failure in coal mining. However, these research results are mainly related to shallow coal mining. With the increase in mining depth, the deepness of most deep coal mines has increased over 600 m. The overburden rock mass will face harsh geological environments, such as high crustal stress, high water pressure, and strong disturbance of mining. Thus, the geo-mechanical environment of deep coal mining has obviously changed, thereby demonstrating special mechanical characteristics of large deformation and strong rheology. All these reasons, the empirical formulas based on data from shallow coal seams are no longer applicable, and it is necessary to deduce new formulas based on data from deep coal mining. On the other hand, the surface observation method used by former researchers cannot guarantee the measurement accuracy because of the long drilling deepness in deep coal mining, the method of in-situ test should be reselected accordingly.

In this work, by referring to the research methods presented in the literature, two common methods for determining the HOFZ in China are introduced as follows: the empirical formula in Chinese Regulations and the in-situ test. And a new method, numerical simulation by orthogonal design (NSOD), have been proposed to determinate the HOFZ in deep coal mining. These three methods were applied to determine the HOFZ of working face No. 111303 in No. 5 coal mine, and compared with the measured HOFZ of in-situ test, the predicted HOFZ of NSOD is more accurate than the HOFZ calculated by the empirical formula. Owing to the in-situ test disadvantages of high cost, difficult construction, and time consuming, the NSOD provides an important reference for predicting the HOFZ in deep coal mining.

2. Two common methods for HOFZ determination

2.1. Empirical formula in Chinese Regulations

In the early 1980s, according to the measured data of HOFZ in north China, an empirical formula (Equation 1) for calculating HOFZ was obtained by regression analysis and recorded in the “Regulations of mining under buildings, water bodies, and railways in China” (herein referred to as “Regulations”).

$$H = \frac{100m}{a \times m + b} \pm c \quad (1)$$

where H is the HOFZ (m), m stands for the total excavating thickness (m), a and b are the coefficients representing different types of roof strata (hard, medium-hard, and weak strata), and c is the standard deviation.

2.2. In-situ test methods

The in-situ test is an extremely important method for determining the HOFZ, and the usual mean is to observe the leakage of water after drilling in the target area. According to the position of the observation boreholes, the in-situ test could be divided into two methods: ground hydrological observation method and underground hydrological observation method. The observation method of the two means is consistent: injecting water into the borehole and sealing for a period of time, and the distribution of rock fractures was evaluated by recording the water leakage. The specific process is described in detail below.

2.2.1. Ground hydrological observation method

Fig. 2 illustrates the ground hydrological observation method. The ground borehole should be set in a position that corresponds to the boundary of goaf. In the process of drilling, the water leakage after injecting water at different drilling depths was recorded; if the drilling depth reaches the upper limb of the fractured zone, then the water leakage will suddenly increase. Finally, the HOFZ could be determined by comprehensive comparison and analysis.

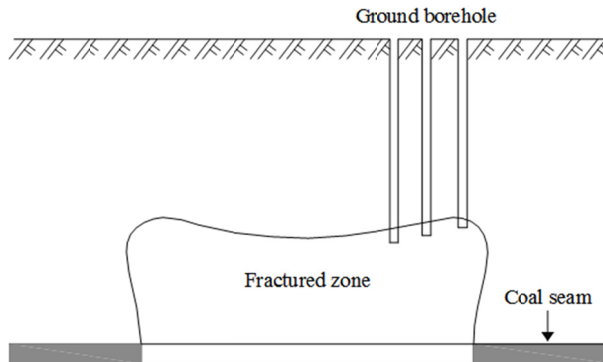


Fig. 2. Sketch of ground hydrological observation method

2.2.2. Underground hydrological observation method

Fig. 3 illustrates the underground hydrological observation method, whose essential feature is to select suitable observation sites around the working face. As shown in Fig. 3, the observation chamber can be dug in the roadway adjacent to the working face and near the cut-out line. Moreover, the device used in the underground hydrological observation method, that is, “underground upward-inclined borehole observation system,” is shown in Fig. 4.

In the process of in-situ test in deep coal mining, the depth of coal seam is more than 600 m from the surface, drilling from the ground to the coal seam is difficult and costly. At the same

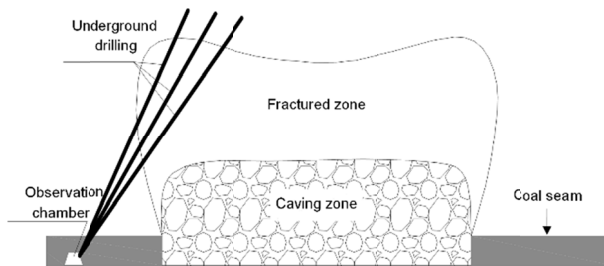


Fig. 3. Sketch of underground hydrological observation method

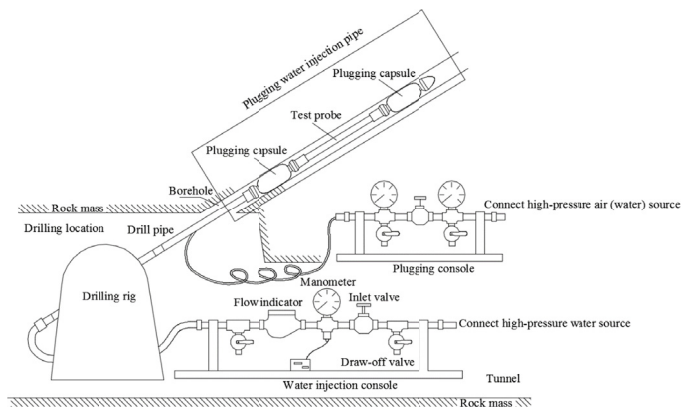


Fig. 4. Underground hydrological observation system

time, the complex strata conditions lead to the observation accuracy of ground hydrological observation is not guaranteed. In contrast, the method of underground hydrological observation is more economical, not only reduces the cost by up to 70% but also provides accurate detection result. Hence, the underground hydrological observation method was chosen in our work.

3. New method for HOFZ determination in deep coal mining

In this work, we have proposed a new method, numerical simulation by orthogonal design (NSOD), to determinate the HOFZ in deep coal mining. The NS refers to the numerical simulation using FLAC3D, while the OD refers to a design method of analyzing the influence degree of representative factors on the research target. A few representative factors with orthogonality, uniformity, dispersion, and comparison are selected from all the influencing factors, and these factors can be compared at multiple levels to find the most important influencing factors.

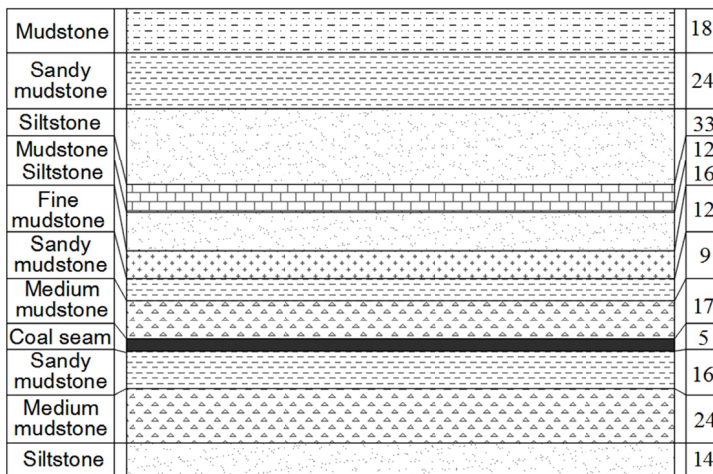
In the process of deep coal mining, the HOFZ is mainly affected by the following four representative factors: coal mining thickness, mining depth, working face width, and dip angle of coal seam. The influence of these factors on the HOFZ can be compared at four levels. According to the NSOD, an orthogonal numerical simulation of four factors and levels was performed using the numerical simulation software.

4. Application of the three methods

4.1. Geological conditions of target coal mine

The working face No. 111303 is the initial working face of No. 13-1 coal seam in No. 5 coal mine. The average thickness of coal is 5.37 m, the length of the working face is 1810 m, the width is 320 m, the average mining depth is 718 m, and the average inclination of coal seam is 7°. The strike of the working face is along the east–west direction with slight topographic relief, and the tendency is to the east-south direction. The overall structure is a monoclinic structure.

As shown in Fig. 5, the overlying strata of the working face are mainly composed of Medium mudstone, sandy mudstone, fine sandstone, and thin coal seam, etc. The immediate roof of the working face is composed of mudstone, with a thickness of approximately 0.12 m-1.13 m and an average thickness of 0.70 m. The middle layers are mostly sandy mudstone, fine sandstone, and thin coal seam. The top layer, which has four aquifers, is composed of a loose bed of Cenozoic soil, with thickness of approximately 568.8 m-610.7 m and an average thickness of 588.9 m.



| | | |
|-----------------|--|----|
| Mudstone | | 18 |
| Sandy mudstone | | 24 |
| Siltstone | | 33 |
| Mudstone | | 12 |
| Siltstone | | 16 |
| Fine mudstone | | 12 |
| Sandy mudstone | | 9 |
| Medium mudstone | | 17 |
| Coal seam | | 5 |
| Sandy mudstone | | 16 |
| Medium mudstone | | 24 |
| Siltstone | | 14 |

Fig. 5. Geological layering of No. 111303 working face

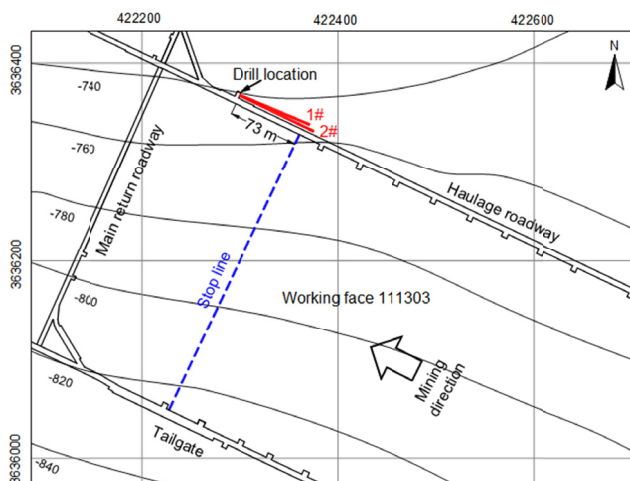
4.2. HOFZ computation using empirical formula in Regulations

The average thickness of coal seam is 5.37 m; hence, $m = 5.37$. Considering that the immediate roof of working face belongs to medium-hard rock strata, we can obtain $a = 1.6$, $b = 3.6$, and $c = 5.6$ according to the Regulations. By incorporating these parameters into empirical formula (1), the computed HOFZ is $H = 41.88 \pm 5.6$ m (maximum height is $H = 47.48$ m).

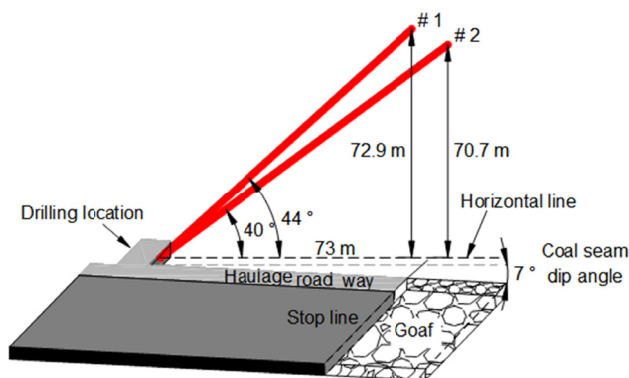
4.3. HOFZ measurement using underground hydrological observation method

4.3.1. Design of the underground hydrological observation method

Fig. 6 shows the layout of the observation boreholes. Two observation boreholes were designed, namely, #1 and #2. The position of the drill hole was designed 73 m from the stop line along the haulage roadway. Based on the past experience of this mine, the highest HOFZ will not exceed 70 m. Therefore, the maximum detection heights of #1 and #2 observation boreholes were designed to be 73 m and 71 m, respectively. The detailed design elements of each borehole are shown in Table 1.



(a) Drill location



(b) Space diagram

Fig. 6. Schematic of the boreholes in working face No.111303

TABLE 1

The parameters of observation boreholes

| Boreholes number | Diameter /mm | Dip angle of borehole /° | Maximum drilling depth /m | Maximum detection HOFZ /m |
|------------------|--------------|--------------------------|---------------------------|---------------------------|
| #1 | 89~94 | 44 | 105 | 72.9 |
| #2 | 89~94 | 40 | 110 | 70.7 |

4.3.2. Analysis of the observational results

According to the geometry shown in Fig. 6b, the HOFZ can be calculated using Equation (2):

$$H = l \cdot \sin \alpha \quad (2)$$

where H is the HOFZ (m), l is the drilling depth corresponding to the sudden change in water leakage (m), and α is the dip angle of borehole (°).

Fig. 7a shows the water leakage of different drilling depths in #1 borehole before and after mining. The water leakage has obviously changed in drilling depth from 64 m to 92 m, which is regarded as critical drilling depth. Before mining, the average water leakage is 8 L/min, which means that original rock crevices exist in the target area. After mining, the average water leakage rapidly changed from 8 L/min to 15 L/min, which means that overlying strata were destroyed, and the original crevices were extended after mining. Simultaneously, the relative variation ratio is less than 1% when drilling was deeper than 92 m, with nearly no change, which means that the rock crevices were undeveloped. By substituting the critical drilling depth (64 m–92 m) and the elevation angle of borehole (44°) into Equation (2), the maximum HOFZ is 63.91 m and the minimum HOFZ is 44.46 m.

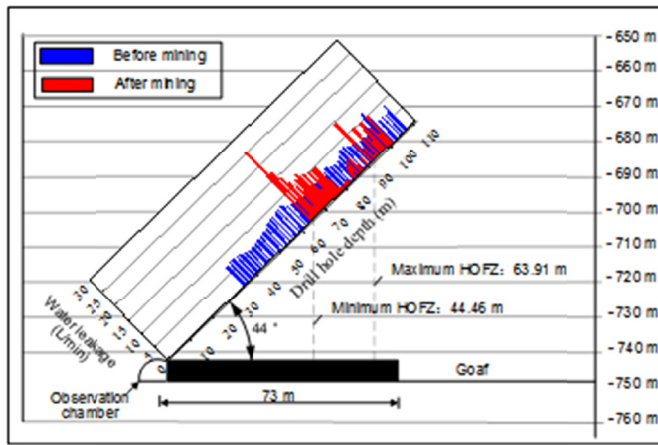
Fig. 7b shows the water leakage of different drilling depths in #2 borehole before and after mining. The water leakage has obviously changed in drilling depth from 43 m to 82 m. Before mining, the average value of water leakage is approximately 13 L/min, which means that original rock crevices exist in the target area. After mining, the water leakage rapidly changed from 13 L/min to 19 L/min, which means that overlying strata were destroyed, and the original crevices were extended after mining. Simultaneously, the relative variation ratio is less than 1% when drilling was deeper than 82 m, with nearly no change, which means that the rock crevices were undeveloped. By substituting the critical drilling depths (43 m–82 m) and the elevation angle of borehole (40°) into formula (2), the maximum HOFZ is 52.71 m and the minimum HOFZ is 27.64 m.

The combination of the measured results of #1 and #2 boreholes determined that the HOFZ of this location is 63.91 m.

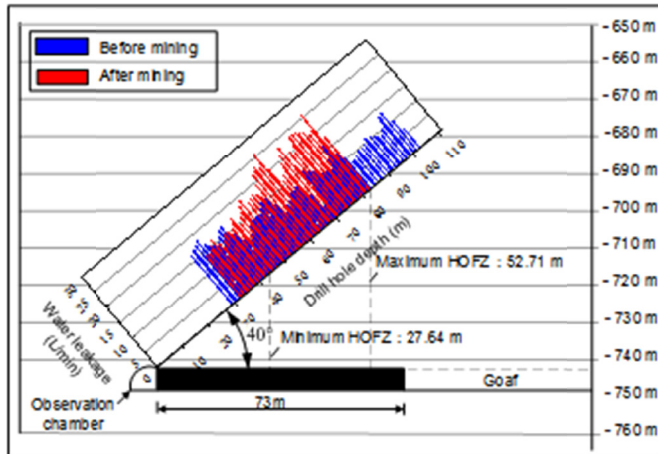
4.4. HOFZ prediction using NSOD

4.4.1. Orthogonal design of the four representative factors

We designed the simulation values of four representative factors according to the geological conditions of target coal mine: The actual mining depth of No. 5 coal mine is 718 m, and the four simulation mining depths were designed at 650, 700, 750, and 800 m. The principle is that the simulation range should include the actual value of this factor. The range of the three other factors was designed on the same principle, and specific simulation scheme is shown in Table 2.



(a) Borehole # 1



(b) Borehole # 2

Fig. 7. Water leakage of observation boreholes before and after mining

TABLE 2

Simulation scheme

| Models Number | Influence factors | | | | HOFZ /m |
|---------------|--------------------------|-----------------|-----------------------|------------------------|----------|
| | Coal mining thickness /m | Mining depth /m | Working face width /m | Coal seam dip angle /° | |
| 1 | 2 | 3 | 4 | 5 | 6 |
| No.1 | 2 | 650 | 180 | 0 | 42 |
| No.2 | 2 | 700 | 240 | 5 | 55 |
| No.3 | 2 | 750 | 300 | 10 | 66 |
| No.4 | 2 | 800 | 360 | 15 | 65 |

TABLE 2. CONTINUED

| 1 | 2 | 3 | 4 | 5 | 6 |
|-------|---|-----|-----|----|-----|
| No.5 | 4 | 650 | 240 | 10 | 53 |
| No.6 | 4 | 700 | 180 | 15 | 56 |
| No.7 | 4 | 750 | 360 | 0 | 82 |
| No.8 | 4 | 800 | 300 | 5 | 86 |
| No.9 | 6 | 650 | 300 | 15 | 88 |
| No.10 | 6 | 700 | 360 | 10 | 95 |
| No.11 | 6 | 750 | 180 | 5 | 83 |
| No.12 | 6 | 800 | 240 | 0 | 86 |
| No.13 | 8 | 650 | 360 | 5 | 107 |
| No.14 | 8 | 700 | 300 | 0 | 98 |
| No.15 | 8 | 750 | 240 | 15 | 83 |
| No.16 | 8 | 800 | 180 | 10 | 94 |

4.4.2. Numerical simulation model

Based on the geological conditions of the target coal mine, the similar strata were divided into the same groups, and 12 groups were also divided (Fig. 5). A total of 16 three-dimensional simulation models were established according to the thickness of the strata in Fig. 5 and the design values of the four representative factors in Table 2. The appearance of these models is consistent, as shown in Fig. 8. External dimensions of these models are all $800\text{ m} \times 600\text{ m} \times 200\text{ m}$. During the simulation process, the vertical constraint is imposed at the bottom of the model, the horizontal constraint is imposed around the model, and the top of the model is set as a free surface, with the vertical load applied on the top surface to simulate the gravity of the overlying strata. Take model No. 16 as an example, $7.9059 \times 10^9\text{ kN}$ loads were applied on the top of the model to simulate the gravity of the 659 m-thick overburden, that is, the 659 m is equal to the model No. 16 mining depth of 800 m minus the 141 m-thick overburden, which was already built in the model. Then, the overlying strata average density was taken as 2550 kg/m^3 , and the gravity acceleration was taken as 9.8 m/s^2 . The models followed the Mohr-Coulomb yield criterion, and the rock mass mechanical parameters used in the simulation were derived from field measurements, as shown in Table 3.

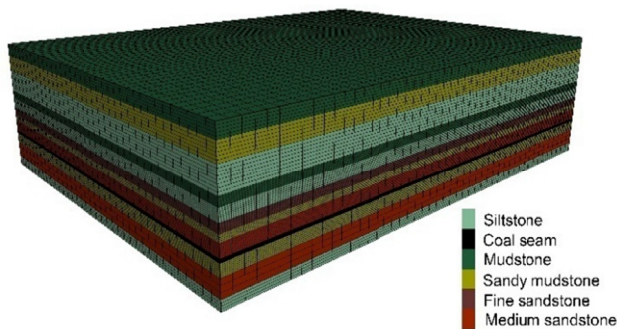


Fig. 8. Appearance schematic of numerical model

TABLE 3

Mechanical parameters of rock mass

| Rock mass | Density /kg · m ⁻³ | Elastic modulus /GPa | Poisson's ratio | Cohesion /MPa | Tensile strength /MPa | Friction angle /° |
|----------------|----------------------------------|-------------------------|--------------------|------------------|--------------------------|----------------------|
| Sandstone | 2400 | 9.4 | 0.21 | 6.0 | 2.4 | 36 |
| Fine sandstone | 2600 | 10.5 | 0.30 | 7.2 | 2.6 | 34 |
| Siltstone | 2700 | 12.5 | 0.35 | 5.2 | 3.6 | 32 |
| Sandy mudstone | 2550 | 10.0 | 0.28 | 5.5 | 2.8 | 35 |
| Mudstone | 2500 | 9.0 | 0.26 | 5.0 | 2.2 | 33 |
| Coal seam | 1500 | 1.3 | 0.23 | 0.55 | 1.6 | 28 |

4.4.3. Analysis of numerical simulation results

(1) Analysis of simulation nephogram

According to the simulation results, the HOFZ was determined based on the range of plastic zone. Take the simulation results of model No. 16 as an analytical sample.

Fig. 9a shows the principal stress nephogram on the middle plane of model No. 16 which is perpendicular to the coal seam strike. The principal stress nephogram can be divided into the following three regions: low-tensile-stress region, stress transition region, and compressive stress region. The bottom layer of the overburden gradually collapsed after coal seam excavation, and the rock mass in this region has low tensile stress state due to the existence of pressure arch. This low-tensile-stress region can be regarded as the caving zone. The upper rock mass above the caving zone is the transition stress region and can be regarded as the fractured zone. Plastic deformation occurred in this region with a high degree of fracture development. The stress state of this region gradually changed from tensile to compressive stress state. The upper rock mass above this region is the compressive stress region and can be regarded as the continuous deformation zone. Elastic deformation occurred in this region, but no plastic deformation occurred.

Fig. 9b shows the shear stress nephogram on the middle plane of model No. 16 which is perpendicular to the coal seam strike. The shear stress concentration occurred at the goaf boundary. Owing to the support of boundary pillar, the rock mass in this region is synchronously affected by tensile and compressive stresses. Simultaneously, with the increase in crustal stress, the maximum shear stress occurred in the lower boundary along the coal seam tendency.

Fig. 9c shows the plastic zone nephogram on the middle plane of model No. 16 which is perpendicular to the coal seam strike. Corresponding to the shear stress distribution, the plastic zone in the goaf boundary is obviously higher than that in the middle part of goaf, and the highest plastic zone occurred in the lower boundary along the coal seam tendency. Consequently, a saddle-shaped plastic zone is formed.

Considering the locations of the boreholes, which were arranged in the high boundary along the coal seam tendency owing to the limitation of construction conditions during the in-situ test, the HOFZ was also determined in the high boundary along the coal seam tendency during the simulation, which can be compared with the in-situ test results. The HOFZ of the 16 models is shown in Table 2.

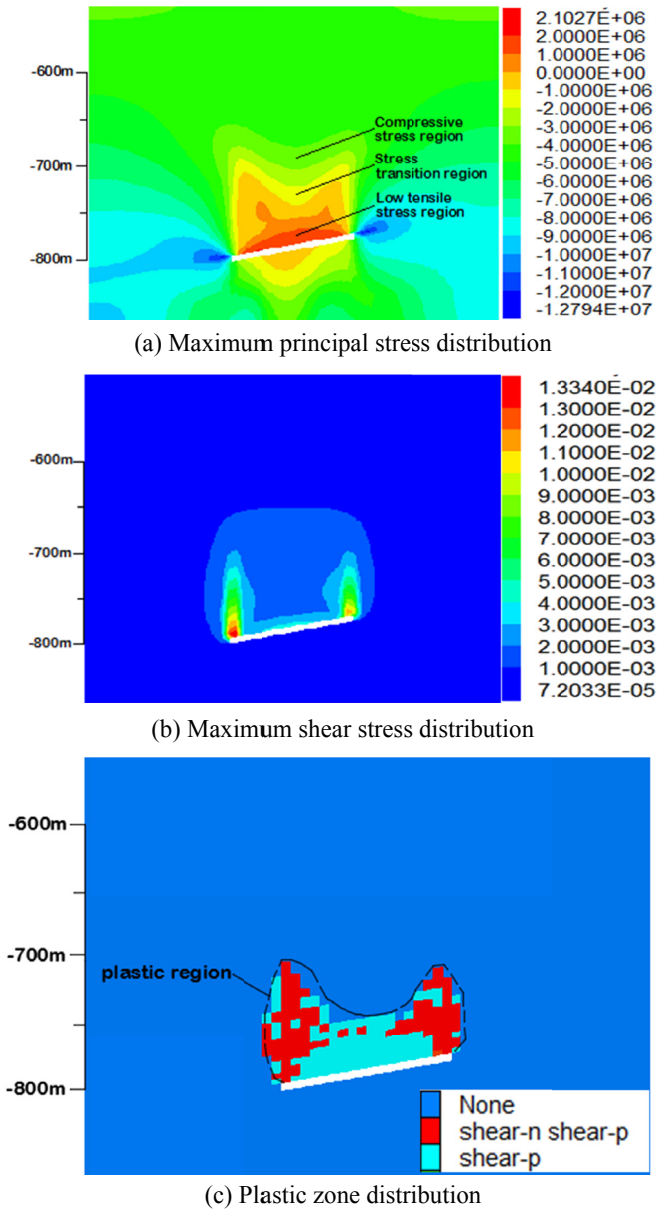


Fig. 9. Simulation results of model No. 16

(2) Predicted formula of the HOFZ

By comparing the four representative factors at different levels, the influence of each factor on HOFZ was analyzed. Roman numerals I-IV were used to show the effect of different levels. Letters *m*, *h*, *d*, and θ indicate the coal mining thickness, mining depth, working face width, and

coal seam dip angle respectively, and R represents the range of each factor. Therefore, the mean values of factor A in four levels can be calculated as follows:

$$\begin{cases} I_m = \text{Average}(42, 55, 66, 65) = 57 \\ II_m = \text{Average}(53, 56, 82, 86) = 69.25 \\ III_m = \text{Average}(88, 95, 83, 86) = 88 \\ IV_m = \text{Average}(107, 98, 83, 94) = 95.5 \end{cases} \quad (3)$$

The value of R was calculated as follows:

$$R_m = \text{Max}(I_m, II_m, III_m, IV_m) - \text{Min}(I_m, II_m, III_m, IV_m) = 95.5 - 57 = 38.5 \quad (4)$$

Therefore, the values of R_h , R_d , and R_θ can be calculated in the same way, and the results are shown in Table 4.

TABLE 4

Range analytical results of the four representative factors

| Mean value of each level and R value | Four representative factors | | | |
|--|-------------------------------|----------------------|----------------------------|----------------------------------|
| | Coal mining thickness $/m$ | Mining depth $/h$ | Working face width $/d$ | Coal seam dip angle $/\theta$ |
| Level I | 57 | 73 | 68.75 | 73 |
| Level II | 69.25 | 76 | 69.25 | 76 |
| Level III | 88 | 78.5 | 84.5 | 78 |
| Level IV | 95.5 | 82 | 87.25 | 82.75 |
| R | 38.50 | 9.00 | 18.50 | 9.75 |

Fig. 10 shows the relationship curve between each representative factor and the HOFZ. By comparing the R values of the four factors, the influence of such factors on HOFZ is listed as follows: coal seam thickness, working face width, coal seam dip angle, and mining depth.

As shown in Fig. 10, the linear correlativity between the HOFZ and the four factors is particularly prominent. Hence, a prediction formula for predicting the HOFZ was established by a linear-regression analysis of the data in Table 2, and the correlation coefficient of regression equation is 0.96. The regression equation is shown as follows:

$$H = 6.7875m + 0.0744h + 0.01156d + 0.305\theta - 59.2 \quad (5)$$

where H is the HOFZ (m), m is the coal mining thickness (m), h is the mining depth (m), d is the working face width (m), and θ is the coal seam dip angle ($^\circ$).

By substituting the parameters ($m = 5.37$, $h = 718$, $d = 320$, $\theta = 7$) of the working face No. 111303 into formula (5), the calculated HOFZ is $H = 69.6$ m.

5. Comparison and analysis of the three methods

The measured HOFZ using in-situ test is $H = 63.91$. The computed HOFZ using the empirical formula in Regulations is $H = 41.88 \pm 5.6$ m (maximum height is $H = 47.48$ m), and the relative

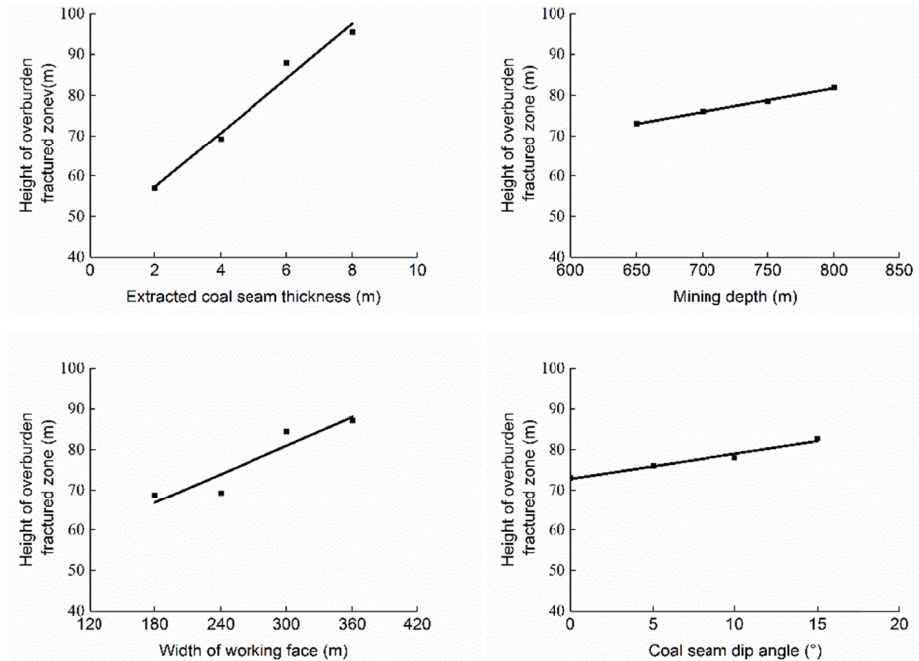


Fig. 10. The relationship curve between the HOFZ and the four representative factors

error is 25.7% with the measured HOFZ. The predicted HOFZ using NSOD is $H = 69.6$ m, and the relative error is 8.9% with the measured HOFZ. The NSOD proposed in this work is more accurate than the empirical formula in Regulations. Evidently, the empirical formula in Regulations is unsuitable for deep mining conditions. Although the in-situ test is accurate, the application is difficult and the cost is high. Compared to the in-situ test, the NSOD is not restricted by bad construction conditions and has a low cost.

6. Conclusions

- (1) In this work, a new method, called NSOD, have been proposed to determinate the HOFZ in deep coal mining. According to the application results, the predicted HOFZ using NSOD is more accurate than that of the empirical formulation in Regulations. The NSOD can be applied in similar mining conditions to save time and money needed for the in-situ test.
- (2) According to the simulation results of NSOD, the principal stress nephogram of overburden after mining can be divided into three regions: low-tensile-stress region, stress transition region, and compressive stress region. The phenomenon of shear stress concentration appears at the boundary of goaf, and the maximum shear stress occurred in the low boundary along the coal seam tendency. Therefore, we proposed the corresponding relationship between stress nephogram and plastic zone nephogram: The highest plastic zone occurred in the boundary of goaf due to the concentration of shear stress.

- (3) The simulation results of NSOD show that the coal mining thickness is the decisive factor affecting the HOFZ in deep coal mining, followed by the working face width, coal seam dip angle, and then mining depth.

Acknowledgments

The research presented in this paper is supported by National Key R&D Program of China (No.2017YFC0804105) and Natural Science Foundation of China (No.51574250).

References

- Singh M.M., Kendorski F.S., 1983. *Strata disturbance prediction for mining beneath surface water and waste impoundments*. Proc. 1st Conference on Ground Control in Mining, Uni. West Virginia **20** (1), 76-89.
- Wang G., Huang W., Sun L., et al. 2016. *High Drilling Methane Drainage in Fracturing Zones Formed by Water Injection into Boreholes*. Archives of Mining Sciences **61** (1), 137-156.
- Miao X.X., Cui X.M., Wang J.A., 2011. *The height of fractured water-conducting zone in undermined rock strata*. Engineering Geology **120** (1-4), 32-39.
- Zhang J., Shen B., 2004. *Coal mining under aquifers in China: a case study*. International Journal of Rock Mechanics and Mining Sciences **41**, 629-639.
- Zhang D., Fan G., Ma L., Wang X., 2011. *Aquifer protection during longwall mining of shallow coal seams: A case study in the Shendong Coalfield of China*. International Journal of Coal Geology **86**, 190-196.
- Xu Z., Sun Y., Dong Q., Zhang G., Li S., 2010. *Predicting the height of water-flow fractured zone during coal mining under the Xiaolangdi Reservoir*. Mining Science and Technology (China) **20**, 434-438.
- Peng S.S., Ma W., Zhong W., 1992. *Surface subsidence engineering*. Society for Mining, Metallurgy, and Exploration.
- Zhou Y., 1991. *Evaluating the impact of multiseam mining on recoverable coal reserves in an adjacent seam*. Virginia Division of Mineral Resources, Commonwealth of Virginia, Department of Mines. Minerals and Energy, Pub.
- Majdi A., Hassani F.P., Nasiri M.Y., 2012. *Prediction of the height of destressed zone above the mined panel roof in longwall coal mining*. International Journal of Coal Geology **98**, 62-72.
- Ghabraie B., Ren G., Zhang X., Smith J., 2015. *Physical modelling of subsidence from sequential extraction of partially overlapping longwall panels and study of substrata movement characteristics*. International Journal of Coal Geology **140**, 71-83.
- Singh G.S.P., Singh U.K., 2009. *A numerical modeling approach for assessment of progressive caving of strata and performance of hydraulic powered support in longwall workings*. Computers and Geotechnics **36**, 1142-1156.
- Sui W., Hang Y., Ma L., Wu Z., Zhou Y., Long G., Wei, L., 2015. *Interactions of overburden failure zones due to multiple-seam mining using longwall caving*. Bulletin of Engineering Geology and the Environment **74**, 1019-1035.
- Xie G.X., Chan, J.C., Yang K., 2009. *Investigations into stress shell characteristics of surrounding rock in fully mechanized top-coal caving face*. International Journal of Rock Mechanics and Mining Sciences **46**, 172-181